Thalamus Degeneration and Inflammation in Two Distinct Multiple Sclerosis Animal Models

Nina Wagenknecht[1] · Birte Becker[1] · Miriam Scheld[1] · Cordian Beyer[1] · Tim Clarner[1] · Tanja Hochstrasser[2] · Markus Kipp[2]

Abstract There is a broad consensus that multiple sclerosis (MS) represents more than an inflammatory disease: it harbors several characteristic aspects of a classical neurodegenerative disorder, i.e., damage to axons, synapses, and nerve cell bodies. While several accepted paraclinical methods exist to monitor the inflammatory-driven aspects of the disease, techniques to monitor progression of early and late neurodegeneration are still in their infancy and have not been convincingly validated. It was speculated that the thalamus with its multiple reciprocal connections is sensitive to inflammatory processes occurring in different brain regions, thus acting as a "barometer" for diffuse brain parenchymal damage in MS. To what extent the thalamus is affected in commonly applied MS animal models is, however, not known. In this article we describe direct and indirect damage to the thalamus in two distinct MS animal models. In the cuprizone model, we observed primary oligodendrocyte stress which is followed by demyelination, microglia/astrocyte activation, and acute axonal damage. These degenerative cuprizone-induced lesions were found to be more severe in the lateral compared to the medial part of the thalamus. In $MOG_{35–55}$-induced EAE, in contrast, most parts of the forebrain, including the thalamus were not directly involved in the autoimmune attack. However, important thalamic afferent fiber tracts, such as the spinothalamic tract were inflamed and demyelinated on the spinal cord level. Quantitative immunohistochemistry revealed that this spinal cord inflammatory-demyelination is associated with neuronal loss within the target region of the spinothalamic tract, namely the sensory ventral posterolateral nucleus of the thalamus. This study highlights the possibility of trans-neuronal degeneration as one mechanism of secondary neuronal damage in MS. Further studies are now warranted to investigate involved cell types and cellular mechanisms.

Keywords Cuprizone · Demyelination · Microglia · Gray matter · White matter · Axonal damage · Neurodegeneration

Introduction

Multiple sclerosis (MS) is known as a complex, multifactorial, polygenic disease, influenced by various factors among age, gender, hormones, viruses, and environment. At present, the most widely accepted hypothesis is that autoreactive T and B cells induce myelin damage, neuroinflammation, and neurodegeneration. However, primary oligodendrocyte dysfunction was implicated as well as potential disease-triggering factor (Barnett and Prineas 2004; Scheld et al. 2016). Despite an unknown etiology, the (*histo*-)pathological hallmarks of MS lesions are well-defined. These include focal and diffuse demyelination, oligodendrocyte loss, inflammation, and neuronal damage which can be seen in various brain regions including diverse white and gray matter areas (Bo et al. 2006; Kipp et al. 2012).

From a clinical point of view, relapsing-remitting MS (RRMS) is the most common disease course affecting about 85 % of all MS patients. RRMS means that symptoms appear (i.e., a relapse) and then fade away either partially or completely (i.e., remitting). Secondary progressive MS (SPMS) is characterized by chronically progressive clinical worsening over time. This progressive course usually follows a period of well-defined RRMS disease course. During the transition from

✉ Markus Kipp
markus.kipp@med-uni-muenchen.de

[1] Institute of Neuroanatomy, Faculty of Medicine, RWTH Aachen University, 52074 Aachen, Germany

[2] Department of Anatomy II, Ludwig-Maximilians-University of Munich, Pettenkoferstrasse 11, 80336 Munich, Germany

RRMS to SPMS, relapse frequency decreases but quickening of neurodegeneration can be observed. In about 15 % of patients, classical relapses from the beginning cannot be clearly delineated, despite clinical deterioration, a disease course called primary progressive MS (PPMS). A PPMS patient's rate of progression may vary over time with an occasional plateau or even temporary improvement, but the overall progression remains continuous (Lublin and Reingold 1996). There is good evidence that the pathological correlate of a relapse is inflammation (i.e., peripheral immune cell recruitment into the brain with subsequent damage to the brain parenchyma), whereas the accumulation of irreversible disability (i.e., disease progression) is due to neuroaxonal pathology including gray matter demyelination, destruction of synapses, axonal damage, or neuronal dystrophy. Results of several studies suggest that the extent of neuroaxonal degeneration is the best predictor for disease progression, much better than white matter pathology (Calabrese et al. 2015; Dutta and Trapp 2014; Kipp et al. 2015). However, underlying mechanisms triggering neuroaxonal degeneration in MS patients are still poorly understood, and imaging techniques to quantify the extent of neuroaxonal loss in MS patients are still in their infancy.

In some neurodegenerative disorders, populations of neurons destroyed by a particular disease are embedded in functional networks. In Alzheimer's disease, as well as in olivo-ponto-cerebellar atrophy, progressive supranuclear palsy, amyotrophic lateral sclerosis (ALS), primary autonomic failure of the Shy-Drager type, and other system degenerations, the main feature of the affected neuronal populations is their anatomical interconnectivity. In principal, three distinct biological phenomena can cause neuronal degeneration after disrupted neuronal connectivity namely (i) anterograde trans-neuronal degeneration, (ii) retrograde trans-neuronal degeneration, or (iii) Wallerian degeneration. To understand the underlying pathophysiology, it is essential to recognize that neurons not only communicate by passing an electrical signal from one to another but at the same time can propagate trophic factors by means of anterograde and retrograde trans-neuronal transport (Ferguson et al. 1990). Trophic factors, such as BDNF or FGF-2, can be released by neurons (Dieni et al. 2012; Figueiredo et al. 2008), and these trophic factors within the synaptic cleft can regulate presynaptic and postsynaptic neuronal function and survival (McCabe et al. 2003; Mosca et al. 2012; Nikoletopoulou et al. 2010). Thus, trophic reciprocal interactions between target neurons and their afferents are thought to regulate neuronal survival and to determine the shape and size of axonal and dendritic processes during development (Purves et al. 1988). In consequence, diffuse neurodegenerative changes might be best studied in brain regions with extensive connectivity. One of these structures is the thalamus.

The thalamus forms the largest part of the diencephalon and is eponymous for other diencephalic components such as the epithalamus and hypothalamus. Although the thalamus may appear to be a maddening jumble of nuclei, three basic types of thalamic nuclei can be distinguished: first relay nuclei, second association nuclei, and third nonspecific nuclei. Relay nuclei receive input from the periphery and forward that information to the cortex (Jones 1991) and can be divided into three functional groups: (i) sensory relay nuclei that receive input from the peripheral sensory receptors through their respective pathways and project to sensory areas of the cortex [ventral posterolateral (VPL), ventral posteromedial (VPM), medial geniculate, and lateral geniculate nuclei; (Berkley 1986)], (ii) motor relay nuclei that interconnect with motor structures and project to motor areas of the cortex [ventral lateral (VL) and ventral anterior (VA) nucleus; (McFarland and Haber 2002; Sommer 2003)], and (iii) limbic nuclei that interconnect with the different structures of the limbic system (anterior nucleus, lateral dorsal nucleus, and dorsomedial nucleus). Association nuclei as the second principal type of thalamic nuclei receive most of their input from the cerebral cortex and project back to the cerebral cortex in the association areas where they appear to regulate activity, among other functions. The pulvinar is the largest of these association nuclei, occupying the posterior part of the dorsal tier of the thalamus (Shipp 2003). The third principal type of thalamic nuclei are the nonspecific nuclei, including many of the intralaminar and midline thalamic nuclei that project quite broadly through the cerebral cortex, and may be involved in general functions such as alerting (Sherman 2007).

Today, it is known that the thalamus is cardinally involved in the MS pathological process. In 1983, Gilbert and colleagues found in two out of five cases small plaques in the thalamus and brain stem (Gilbert and Sadler 1983). Twenty-five years later, Vercellino and colleagues performed a systematic neuropathological study focusing on the structural deep gray matter (i.e., caudate, thalamus, putamen, pallidum, hypothalamus, amygdala, and claustrum) in MS (Vercellino et al. 2009). They found that deep gray matter demyelination can be frequently observed in post-mortem MS brains. Besides demyelination and inflammation, the authors observed clear signs of neurodegeneration, including neuronal loss, neuronal shrinkage, and acute axonal damage, the latter evidenced by anti-amyloid precursor protein (APP) immunohistochemistry. These findings are in agreement with another study from Cifelli and colleagues. They additionally observed that neuronal loss might be the substrate for thalamic atrophy (Cifelli et al. 2002). Besides pathological studies, clinical studies underpin the assumption that the thalamic network is severely impaired in MS patients. Findings include the reduction of cerebral blood flow (Inglese et al. 2007; Ota et al. 2013; Rashid et al. 2004), a decrease of normalized thalamic volume (Cifelli et al. 2002; Houtchens et al. 2007), or reduced cerebral glucose metabolism rate (Blinkenberg et al. 2000; Derache et al. 2006). Due to its great connectivity, damage to the thalamus and its connections potentially impairs a wide range of

neurologic functions that may clinically translate into significant cognitive, physical, or mental disability (Minagar et al. 2013). To be more specific, atrophy of the thalamus, determined with MRI, can help identify which patients with clinically isolated syndrome (CIS) are at risk for developing clinically definite MS (Brex et al. 2000; Calabrese et al. 2011; Zivadinov et al. 2013). Second, it was found that atrophy in the cortex and subcortical deep gray matter, including the thalamus, was significantly related to patients' declining cognitive abilities. Thus, thalamus atrophy is a strong predictor for cognitive decline in MS patients (Batista et al. 2012; Benedict et al. 2013; Houtchens et al. 2007; Schoonheim et al. 2012). Furthermore, thalamic atrophy is correlated with long-term accumulation of EDSS-rated clinical disability in patients with MS (Magon et al. 2014; Rocca et al. 2010). In summary, the thalamus is an important structure in the context of MS-related disability and disease progression.

Our knowledge regarding the involvement of the thalamus in MS animal models is sparse. In this study, we aimed to analyze thalamus involvement in the autoimmune animal model for MS (i.e., experimental autoimmune encephalomyelitis (EAE)) (Stromnes and Goverman 2006) and the toxic MS animal model cuprizone (Kipp et al. 2009). Furthermore, we addressed to what extent degeneration/demyelination of thalamic afferent fiber tracts is paralleled by neurodegeneration of the thalamus.

Materials and Methods

Cuprizone-Induced Demyelination

C57BL/6J mice were obtained from Janvier (France) and kept under standard laboratory conditions according to the Federation of European Laboratory Animal Science Association's recommendations. The procedures were approved by the Review Board for the Care of Animal Subjects of the district government (Nordrhein-Westfalen, Germany) and performed according to international guidelines on the use of laboratory mice. Demyelination was induced by feeding 10-week-old (19–21 g), male mice with ground standard rodent chow containing 0.25 % cuprizone (bis-cyclohexanone oxaldihydrazone, Sigma-Aldrich Inc., Germany) for the indicated period, as published previously (Clarner et al. 2015; Slowik et al. 2015). Control mice were fed ground standard chow.

Induction of EAE and Clinical Scoring

For induction of EAE, we used a commercially available kit from Hooke Laboratories (EK-2110; Lawrence, MA 01843, USA). In brief, at day 0, 100 μl of an emulsified Freund's adjuvant solution containing 1 mg/ml $MOG_{35–55}$ peptide and 5 mg/ml killed mycobacterium tuberculosis H37Ra was injected subcutaneously on the upper and the lower back (100 μl at each position) of 10-week-old female mice. At days 0 and 1, animals additionally received intraperitoneally 100 μl of a pertussis toxin solution (5 μg/2.5 ml dissolved in PBS). For clinical scoring, we used the following grading system: score 0.5 was given when picked up by base of tail, the tail has tension except for the tip. Muscle straining is felt in the tail, while the tail continues to move; score 1.0 was given when picked up by base of tail, instead of being erect, the whole tail drapes over finger. Hind legs are usually spread apart. No signs of tail movement are observed; score 1.5 was given when picked up by base of tail, the whole tail drapes over finger. When the mouse is dropped on a wire rack, at least one hind leg falls through consistently. Walking is very slightly wobbly; score 2.0 was given when picked up by base of tail, the legs are not spread apart, but held closer together. When the mouse is observed walking, it has a clearly apparent wobbly walk. One foot may have toes dragging, but the other leg has no apparent inhibitions of movement; score 2.5 was given when both hind legs have some movement, but both are dragging at the feet (mouse trips on hind feet); Score 3.0 was given when there is limp tail and complete paralysis of hind legs; score 3.5 was given when the mouse is moving around the cage, but when placed on its side, is unable to right itself. Hind legs are together on one side of body; score 4.0 was given when the mouse is minimally moving around the cage but appears alert and feeding.

All animals with a disease score greater than 2.5 received daily 500 μl of Ringer solution by subcutaneous injection. If animals reached at two consecutive days a score of 4, euthanasia was performed, and the animal excluded from any subsequent analyses.

Tissue Preparation, Immunohistochemistry, and Evaluation

Preparation of tissues was performed as previously described with some minor modifications for spinal cord tissues. For histological and immunohistochemical studies, mice were transcardially perfused with 3.7 % paraformaldehyde in phosphate-buffered saline (PBS; pH 7.0–7.4). After overnight post-fixation in the same fixative, brains were dissected, embedded in paraffin, and then coronary sectioned into 5-μm-thick slices. For demineralization of the vertebrae, muscles and connective tissues were carefully removed from the backbone and tissue blocks incubated in 20 % Na-EDTA solution (in aqua dest.) for 48 h at 37 °C, with replacement of Na-EDTA after 24 h. Embedding in paraffin was subsequently performed in the same way as brain tissues. For immunohistochemistry, sections were placed on silane-coated slides, deparaffinized, rehydrated, if necessary heat-unmasked in either citrate or Tris/EDTA-buffer, blocked with PBS containing

1 % normal horse or goat serum, and incubated overnight at 4 °C with the primary antibodies diluted in blocking solution. Primary antibodies and dilutions used in the study are reported elsewhere (Clarner et al. 2015; Schmidt et al. 2013; Slowik et al. 2015). After washing and blocking of endogenous peroxidase with 0.3 % hydrogen peroxide (in PBS) for 30 min, sections were incubated with appropriate biotinylated secondary antibodies for 1 h at room temperature, followed by peroxidase-coupled avidin-biotin-complex (ABC kit, Vector Laboratories). The di-amino-benzidine-reaction (DAB; DAKO Deutschland GmbH, Germany) was used to visualize peroxidase-avidin-biotin complexes. Sections were counterstained with standard hematoxylin to visualize cell nuclei, if appropriate. To verify that stains are specific, negative control experiments (omission of primary antibody and, if appropriate, application of isotype controls) was routinely performed.

The forebrain was analyzed on the level R315 according to the mouse brain atlas published by Sidman et al. The spinal cord was analyzed at the cervical, thoracal, lumbal, and sacral level. Sections in these regions were randomly selected. Stained sections were analyzed using a Nikon ECLIPSE E200 microscope. To estimate myelination in the defined regions of interest, anti-proteolipid protein (PLP) staining intensity has been quantified using ImageJ (NIH; version 1.47v) after automatic setting of a threshold. For quantification of microgliosis, astrocytosis or oligodendrocyte density, cell numbers of two consecutive sections per mice were evaluated, and averaged. $IBA1^+/GFAP^+/OLIG2^+$ cells were only counted when a cell nucleus was clearly visible, considering false positive or negative results due to hypertrophy or shrinkage, respectively. Cell numbers are always given in cells per square millimeter (mm^2). To estimate the extent of acute axonal damage in the region of interest, slides were processed for immunohistochemistry using anti-APP antibodies, which is a frequently used marker to detect acute axonal damage (Bitsch et al. 2000; Herrero-Herranz et al. 2008). Following the same strategy as for quantification of microgliosis, the extent of acute axonal damage was quantified in a blinded and unbiased approach. In this case, APP^+-spheroids were just counted if not localized around a cell nucleus.

For the semi-quantification of demyelination in the different spinal cord segments, Luxol-fast-blue/periodic acid–Schiff (LFB/PAS) stains have been performed, and the extent of demyelination was graded in a blinded manner with 0 = normal myelination, 1 = moderate demyelination, 2 = intermediate demyelination, and 3 = complete demyelination (see Fig. 4 for representative images). To quantify the number of neurons within the sensory thalamus (i.e., within the VPL nucleus), a systematically-randomly sampled (SRS) series of 5-μm-thick brain sections encompassing the entire VPL nucleus of both sides was prepared, and every tenth section was subsequently stained for the pan-neuronal marker protein NeuN following the procedure described above. Stained brain sections were scanned, the VPL outlined using NDP.view2 software (Hamamatsu Photonics, Japan), and cell profiles counted in a blinded approach.

Statistical Analysis

Differences between groups were statistically tested using GrapPad Prism 5. Differences between groups were tested with unpaired *t* test. In case variances were significantly different, Welch's correction was performed. Significance levels are indicated as $*p < 0.05$; $**p < 0.01$; $***p < 0.001$.

Results

Cuprizone Intoxication Induces Demyelination and Axonal Degeneration Within the Thalamus

In the cuprizone model, demyelination occurs due to a primary metabolic disturbance of mature oligodendrocytes (Kipp et al. 2009; Skripuletz et al. 2011). Since this model harbors several similarities with early MS lesions (Barnett and Prineas 2004; De Groot et al. 2001; Lucchinetti et al. 2000; Marik et al. 2007), we decided to evaluate the vulnerability of the thalamus in this particular model. To this end, animals were fed cuprizone for 5 weeks, and myelination (anti-PLP), microgliosis (anti-IBA1), and astrocytosis (anti-GFAP) were compared to control groups which received normal chow during the experimental period.

As shown in Fig. 1, myelination of medial parts of the thalamus, laying medial to the fasciculus retroflexus (arrow in Fig. 1 (a)) and mamillothalamic tract (arrowhead in Fig. 1 (a)), is very low already in control animals. This part was, therefore, excluded from all analyses. Furthermore, by gross inspection of anti-IBA1-stained sections, it was obvious that medial and lateral parts of the thalamus display a different vulnerability against the 5-week cuprizone intoxication period. We, thus, decided to separately evaluate medial and lateral parts of the thalamus (see red dotted line in Fig. 1 (a) for the virtual border between medial and lateral aspects of the thalamus).

As demonstrated in Fig. 1, severe and widespread demyelination could be found within the murine thalamus after a 5-week cuprizone exposure period. Interestingly, vulnerable regions included different functional nuclei among those devoted to motor systems (i.e., ventral anterior-lateral complex, not shown in Fig. 1) or sensory systems (ventral posterolateral nucleus and ventral posteromedial nucleus, see star in Fig. 1 (b)). Demyelination was as well evident in regions not directly related to motor or sensory systems such as in different intralaminar nulcei (for example in the parafascicular nucleus which surrounds the fasciculus retroflexus), or in the posterior complex (rhomb in Fig. 1 (b); see Fig. 2 (d) for an anatomical

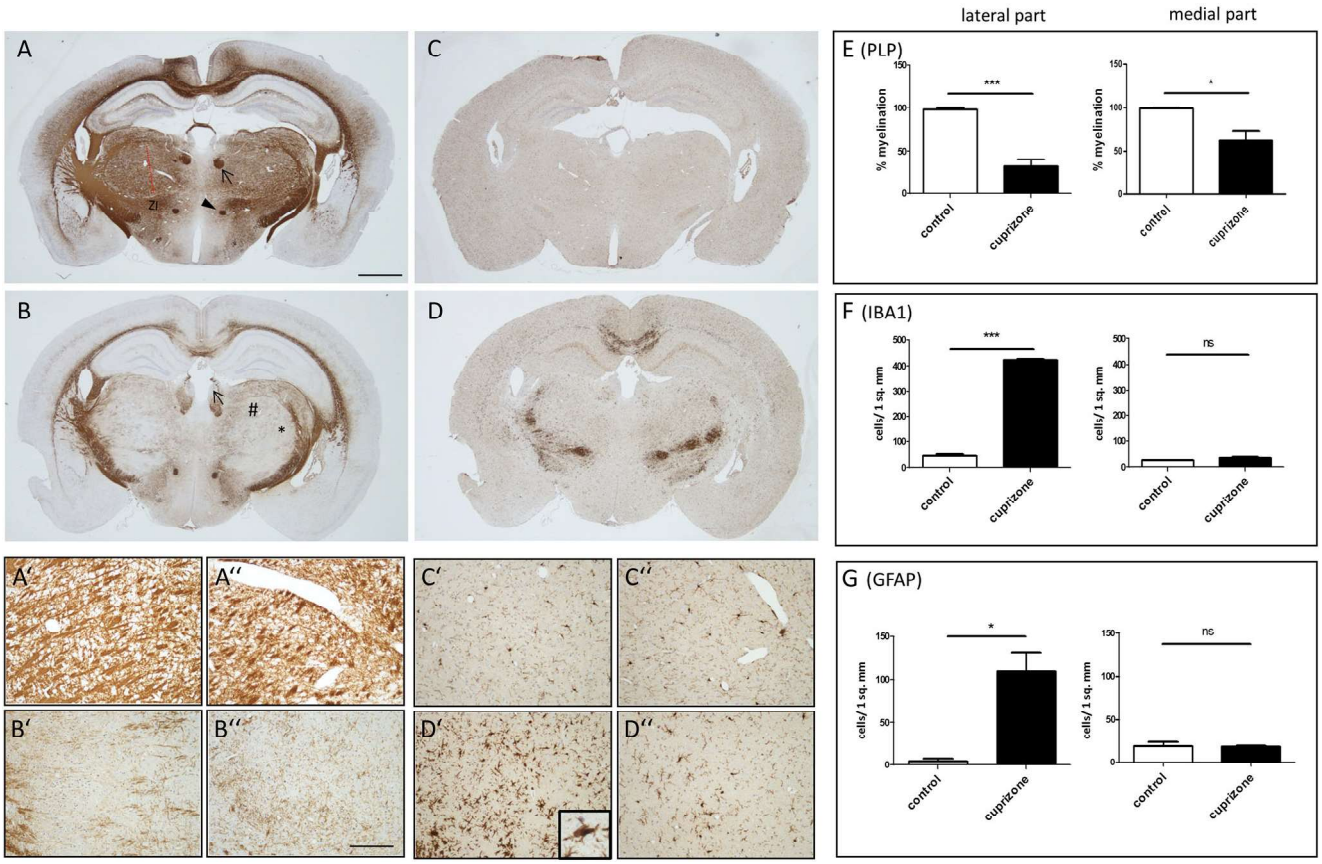

Fig. 1 Cuprizone intoxication induces demyelination of the thalamus. Effect of cuprizone on myelination and reactive gliosis of the thalamus in male mice demonstrated by means of anti-PLP, anti-IBA1, and anti-GFAP immunohistochemistry. An anti-PLP staining of a control mouse on the level of the interbrain (i.e., diencephalon) (*a*). The virtual border between medial and lateral aspects of the thalamus on that level is illustrated by the *red dotted line*. The *arrow* in *a* highlights the fasciculus retroflexus; the *arrowhead* in *a* highlights the mamillothalamic tract. An anti-PLP staining of a mouse treated 5 weeks cuprizone (0.25 %) (*b*). The *arrow* highlights the habenulae region; directly beneath are running fiber tracts of the fasciculus retroflexus. The *star* highlights the location of the sensory VPL/VPM area; the *rhomb* highlights the lateral posterior nucleus of the thalamus. Note widespread demyelination in the thalamus; medial and lateral aspects are affected. An anti-IBA1 staining of a control mouse on the level of the interbrain (i.e., diencephalon) (*c*). An anti-IBA1 staining of a mouse treated 5 weeks cuprizone (0.25 %) (*d*). Quantification of demyelination and microgliosis in the medial and lateral aspect of the thalamus is shown in *e* and *f*, respectively. Note that demyelination is paralleled by graded microglia activation. Lateral thalamic parts of the respective stain in higher magnification (*a'*, *b'*, *c'*, *d'*); medial thalamic parts of the respective stain in higher magnification (*a''*, *b''*, *c''*, *d''*). Quantification of astrocyte activation in the medial and lateral aspect of the thalamus is shown in *g*. *VPL* ventral posterolateral nucleus, *VPM* ventral posteromedial nucleus. Indicated significance levels: $*p \leq 0.05$; $**p \leq 0.01$; $***p \leq 0.001$

overview of the thalamus). Blinded evaluation revealed that the extent of demyelination was more severe in lateral compared to medial parts of the thalamus (Fig. 1 (e)). Demyelinated regions displayed clear signs of microglia activation. In control animals, IBA1$^+$ cells were regularly found to have a small cell body with thin-ramified cell processes (i.e., characteristics of resting microglia cells, see Fig. 1 (c′, c″)). In contrast, the cell body and processes of IBA1+ cells were swollen, and ramification was less pronounced after a 5-week cuprizone exposure period. In line with the finding of more severe demyelination in lateral parts of the thalamus, microglia activation was more pronounced in lateral compared to medial parts (Fig. 1 (f)). Beyond, a significant increase in GFAP$^+$ cell numbers was found in the lateral aspect of the thalamus, indicating activation of the astrocyte population (Fig. 1 (g)). Astrocyte activation was not evident in the medial part of the thalamus.

In MS patients, demyelination of the thalamus was found to be paralleled by acute axonal damage (i.e., component of the neurodegenerative aspect of the disease) (Vercellino et al. 2009). Immunohistochemical visualization of amyloid precursor protein$^+$ (APP$^+$) axonal swellings is a frequently used method to quantify acute axonal damage. We, thus, applied this method to see whether or not demyelination and microglia activation within the thalamus is paralleled by neurodegeneration in the cuprizone model. We focused in this part of the study on lateral aspects of the thalamus because (i) miocrogliosis was found to be most severe there, and (ii) this part of the thalamus harbors important structures relevant for motor and sensory function (i.e., VL, VA, VPL, and VPM).

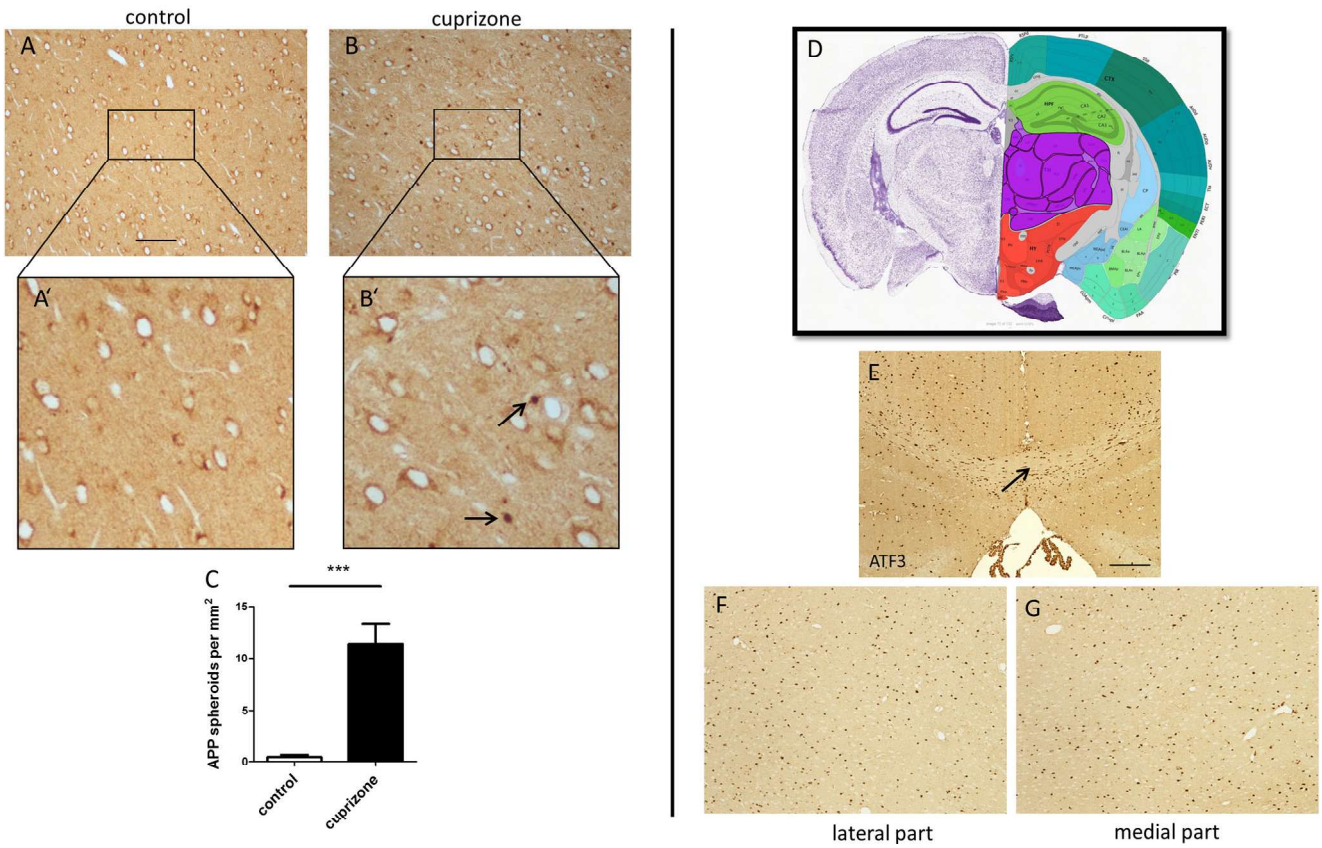

Fig. 2 Cuprizone intoxication induces acute axonal damage and widespread thalamic oligodendrocyte stress. An anti-APP staining of a control mouse on the level of the interbrain (i.e., diencephalon) (*a*). An anti-APP staining of a mouse treated 5 weeks cuprizone (0.25 %) (*b*). The respective areas in a higher magnification (*a′*, *b′*). The *arrows* in *a′* indicate APP-protein in the neuronal cell body. The *arrows* in *b′* highlight APP^+ axonal spheroids, which indicate acute, ongoing axonal damage. The quantification of APP^+ axonal spheroids in the lateral part of the thalamus (*c*). Note significant axonal damage after a 5-weeks cuprizone intoxication period. The anatomical structure of the thalamus at the investigated brain level (shown in *purple*) (*d*). The expression of ATF3 (oligodendrocyte stress marker protein) after 4 days of cuprizone intoxication (*e*–*g*). The *arrow* in *e* highlights the white matter tract *corpus callosum*. Note widespread expression of ATF3 in the medial and lateral aspect of the thalamus, indicating primary oligodendrocyte stress reaction. Indicated significance levels: $*p \leq 0.05$; $**p \leq 0.01$; $***p \leq 0.001$

As shown in Fig. 2, APP^+ material was mainly found in the perinuclear region of neurons in control animals (see arrowheads in Fig. 2 (a′)). The same APP staining pattern was evident in cuprizone-treated animals. In addition, APP^+ spheroids, which have no spatial relation to neuronal cell bodies, were found in the thalamus of cuprizone intoxicated animals (see arrows in Fig. 2 (b′)). Such spheroids were not observed in control animals indicating that acute axonal damage occurs in the thalamus after acute cuprizone-induced demyelination.

Our group was previously able to show that the stress-related protein activating transcription factor-3 (ATF3) is selectively expressed by oligodendrocytes in the cuprizone model (Goldberg et al. 2013). To verify that oligodendrocytes within the thalamus are directly stressed in this model, ATF3 levels were visualized by means of immunohistochemistry. As shown in Fig. 2 (e), numerous $ATF3^+$ cells were found in the white matter tract corpus callosum, which is a well investigated and characterized region in this animal model (Kipp et al. 2011; Skripuletz et al. 2013, 2015). Additionally, we found numerous ATF3-expressing cells in the medial and lateral parts of the thalamus (Fig. 2 (f, g)). To conclude, cuprizone directly attacks oligodendrocytes within the thalamus and, in consequence, induces demyelination, gliosis, and acute axonal damage.

Inflammatory Lesions Are Absent in the Forebrain of $MOG_{35–55}$-Induced EAE

In a next step, we were interested whether the thalamus is as well involved in the disease process if using an autoimmune mediated demyelination model. To this end, female C57BL6 animals were immunized with $MOG_{35–55}$ peptide (for details, see "Material and Methods" section) and sacrificed at either the peak of the disease (i.e., active EAE) or during the chronic disease stage (i.e., chronic EAE). This model is clinically characterized by transient ascending hind limb paralysis and histologically by perivascular mononuclear-cell infiltration in the brain

(mainly cerebellum) and spinal cord with adjacent areas of acute and chronic demyelination. In our experiments, mice immunized with $MOG_{35–55}$ peptide in CFA usually began to show neurological deficits between days 8 and 10, reached peak severity between days 12 and 15, and continued to have substantial deficits throughout the observation period (see Figs. 3a and 5a). CFA + PTX control mice showed no clinical neurological deficits (data not shown).

The first cohort of animals was used to investigate histopathological alterations during the *acute* phase of the disease. As shown in Fig. 3a, in this set of experiments, first clinical symptoms were evident around day 9 and progressively worsened till day 15 post-immunization (i.e., peak of the disease). Histological analyses of the spinal cord revealed subpial, perivascular, and parenchymal mononuclear-cell infiltration into the spinal cord white matter. Peripheral immune cell recruitment was paralleled by demyelination, as demonstrated by a loss of LFB reactivity (Fig. 3b). Furthermore, these areas displayed pronounced accumulation of $IBA1^+$ microglia and macrophages. Such inflammatory foci were found within the dorsal (or posterior) column, lateral column and ventral (or anterior) column. As already reported by other groups (Ruffini et al. 2013; Soulika et al. 2009) a significant number of axons displayed signs of acute axonal damage in inflammatory demyelinated lesions (Fig. 3b). Such histological alterations were absent in CFA + PTX control mice (not shown).

We next were interested about the spatial distribution of *forebrain* lesions in the acute phase of $MOG_{35–55}$-induced EAE. To this end, we analyzed the presence and spatial distribution of perivascular infiltrates (examples are shown in Fig. 3c), being the histopathological correlate for peripheral immune cell recruitment (Scheld et al. 2016). As shown in Fig. 3c, perivascular infiltrates were not found in control nor

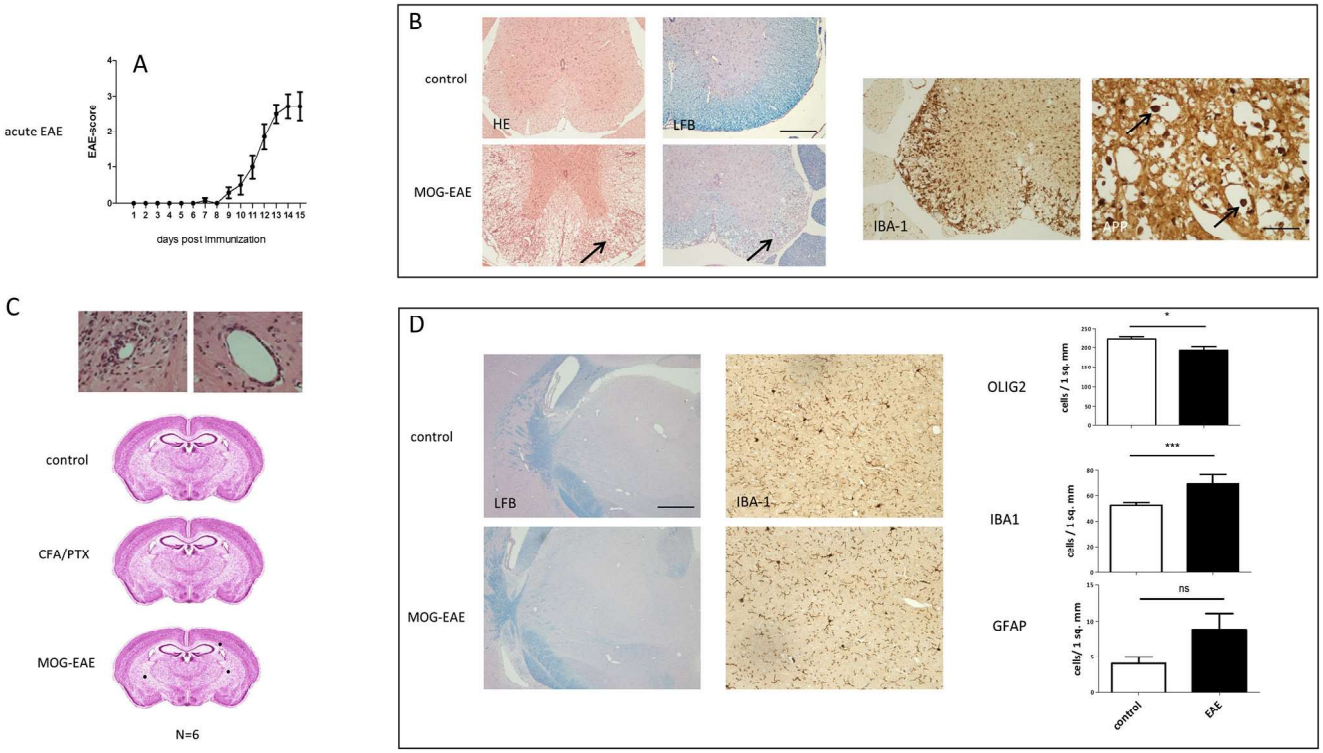

Fig. 3 $MOG_{35–55}$-induced EAE does results in inflammatory spinal cord but not thalamus lesions. **a** EAE clinical disease score in C57BL/6 mice immunized with $MOG_{35–55}$ peptide (see "Material and Methods"). The mean daily disease grade for each group ($n = 6$ mice per group) is shown. In these experiments, the first clinical symptoms were evident around day 9 and progressively worsened till day 14–15 post-immunization (i.e., peak of the disease). At this time point, the animals were sacrificed. **b** Representative HE and LFB/PAS stains of the spinal cord in control (*upper row*) and EAE-diseased animals (*lower row*). *Arrows* in both stains indicate inflammatory-demyelinated lesions. These lesions are, in this animal, located in the antero-lateral funiculus of the spinal cord white matter. From the same region, representative anti-IBA1 and anti-APP stains are shown to visualize monocyte/microglia reactivity and acute axonal damage, respectively. *Arrows* in the anti-APP stain highlight acute, ongoing axonal damage in demyelinated spinal cord lesions. **c** The distribution of perivascular inflammatory infiltrates in the forebrain on the level of the thalamus. The appearance of two representative perivascular inflammatory infiltrates in HE-stained sections is shown in the upper part of **c** (adopted by Scheld et al. from J Neurosci. 2016 Jan. 27;36(4):1410–5). Note that perivascular infiltrates were not found in control nor CFA + PTX control mice. In $MOG_{35–55}$-immunized animals, just three perivascular infiltrates were found at the investigated level of six diseased animals. None of these three infiltrates were located within the thalamus. **d** Histopathological alterations of the thalamus in EAE vs. control animals. Anti-OLIG2, anti-IBA1, and anti-GFAP antibodies were used to visualize oligodendrocytes, microglia/macrophages, and astrocytes, respectively. *CFA* complete Freund's adjuvant), *PTX* Pertussis toxin. Indicated significance levels: $*p \leq 0.05$; $**p \leq 0.01$; $***p \leq 0.001$

CFA + PTX control mice. In $MOG_{35–55}$-immunized animals which developed EAE, just three perivascular infiltrates were found at the investigated level of six diseased animals. None of these three infiltrates were located within the thalamus (compare with Fig. 2 (d) for anatomical borders of the thalamus). Furthermore, we addressed myelination (LFP/PAS), oligodendrocyte cell numbers (anti-Olig2), astrocytosis (anti-GFAP), and microgliosis (anti-IBA1) in the thalamus. We found no overt demyelination of the thalamus in any of the EAE-induced animals. However, numbers of $OLIG2^+$ oligodendrocytes were found to be slightly lower in the thalamus of EAE-diseased animals (224.5 ± 33.5 (mean ± std. deviation) in control animals vs. 193 ± 67.3 in EAE animals; $p = 0.0353$). This decline in oligodendrocyte cell numbers was paralleled by a slight but significant increase in microglia cell numbers. Beyond, numbers of $GFAP^+$ astrocytes tended to be higher in EAE animals (compare Fig. 3d). Thus, while we found no evidence that immune cells directly invade the parenchyma of the thalamus in $MOG_{35–55}$-induced EAE (no perivascular infiltrates; no $CD3^+$ lymphocytes, not shown) subtle alterations were observed with respect to oligodendrocyte cell numbers and microglia/astrocyte activation status.

Neurodegeneration in the Thalamus After Chronic $MOG_{35–55}$-Induced EAE

As pointed out in the "Introduction", trans-neuronal degeneration might contribute to diffuse neurodegeneration in MS and the thalamus might especially be prone for such degenerative processes. Since the thalamus is not affected in the applied EAE model, but important thalamic afferent pathways are demyelinated (such as the sensory spinothalamic tract in the spinal cord), we were interested whether inflammatory lesions located within the spinal cord induce degenerative changes in the sensory part of the thalamus (i.e., the VPL). To this end, a separate cohort of animals was immunized with $MOG_{35–55}$ and sacrificed during the chronic phase of the disease (i.e., around 8 weeks post-immunization). As shown in Fig. 5a, this cohort of animals as well displayed a typical $MOG_{35–55}$ EAE disease course with EAE onset around 9 to 10 days after immunization, and with peak of disease 3 to 5 days after onset for each mouse. The peak of disease lasted 2 to 4 days, followed by partial recovery. Thereafter, there was clinically a stable disease till week 8 (i.e., end of the observation period).

First, we determined the presence or absence of demyelination in the lateral and anterior funiculus which harbor the lateral and anterior spinothalamic tract, respectively. Since these are secondary sensory neurons (i.e., second-order fibers) which have already made synaptic connections with the primary sensory neurons of the peripheral nervous system in the posterior horn of the spinal cord, both fiber bundles directly project towards the sensory part of the thalamus (i.e., towards the sensory VPL). Furthermore, the posterior funiculus of the spinal cord was included in the analysis albeit these are first-order fibers and, thus, do not directly make connections with the sensory part of the thalamus. Extent of demyelination and inflammation was graded in the respective white matter parts of the spinal cord in LFB/PAS-stained slides with 0 = normal myelination/no inflammation, 1 = moderate demyelination/inflammation, 2 = intermediate demyelination/inflammation, and 3 = complete demyelination/severe inflammation (see Fig. 4 for representative pictures).

As shown in Fig. 5b, c, all three sensory pathways displayed significant demyelination/inflammation on all four investigated spinal cord levels (i.e., cervical, thoracal, lumbal, and sacral). Demyelination in the anterior (green arrowheads) and lateral (yellow arrowheads) funiculus was mainly observed at superficial white matter layers, however, regularly involved the entire width of the spinal cord white matter. The dorsal funiculus (red arrowheads), if affected, was usually not entirely demyelinated, but demyelination and inflammation was mainly found within the parts containing the tract of Goll (i.e., fasciculus gracilis). In most cases, demyelination was moderate with an average score of 1–1.2 (see Fig. 5b).

Together with the results obtained after acute EAE, it is clearly evident that afferent projections to the thalamus are subjected to inflammatory demyelination in this model. To see whether or not the thalamus displays neuronal loss, we quantified the number of neurons in the sensory thalamus. Neurons were visualized with immunohistochemistry using antibodies directed against the pan-neuronal marker protein NeuN, and cell numbers and density were analyzed in the VPL nucleus, which directly receives projections from the anterior and lateral spinothalamic tract. In case lesions within these fiber tracts on the level of the spinal cord induce transneuronal degeneration (i.e., dying forward), one would

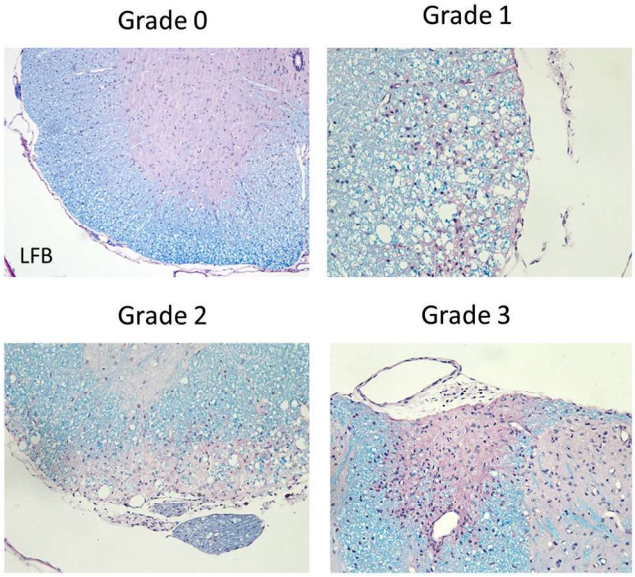

Fig. 4 Grading scheme for demyelination and inflammation in the spinal cord of chronic EAE-diseased animals

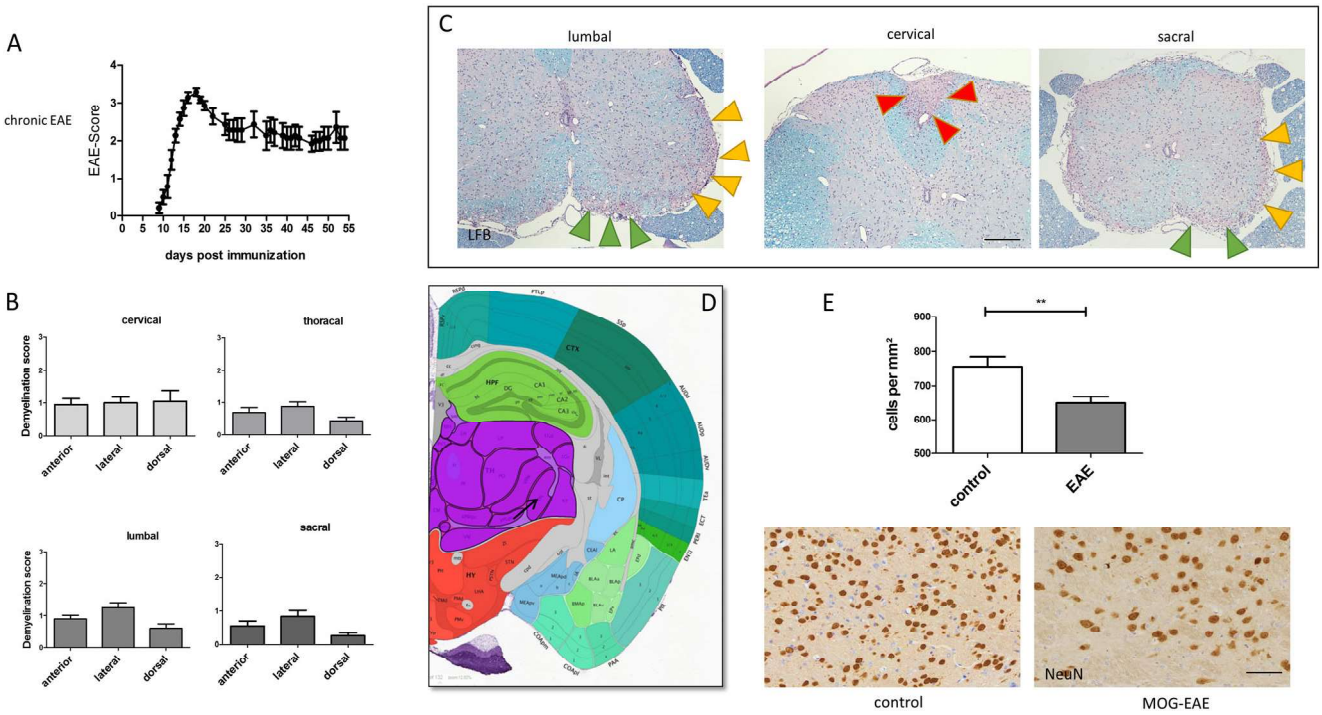

Fig. 5 Transneuronal thalamus degeneration in chronic $MOG_{35–55}$-induced EAE. **a** EAE clinical disease score in C57BL/6 mice immunized with $MOG_{35–55}$ peptide (see "Material and Methods"). The mean daily disease grade for each group ($n = 6$ mice per group) is shown. Animals were sacrificed after chronic EAE. **b** The mean severity of demyelination and inflammation within the anterior, lateral, and dorsal funiculus of the spinal cord white matter. For grading examples, please see Fig. 4. Note that all three white matter parts of the spinal cord are affected at all investigated levels. **c** Representative appearance of these lesions after chronic $MOG_{35–55}$-induced EAE. *Arrow* in **d** The anatomical location of the sensory ventral posterolateral nucleus (i.e., VPL). **e** Quantification of neuronal cell numbers evaluated in control ($n = 3$) and EAE-diseased animals ($n = 6$). Quantification was performed in anti-NeuN-stained sections following criteria of design-based stereology. Note significant neuronal loss in the ventral posterolateral nucleus after chronic EAE. Indicated significance levels: $*p \leq 0.05$; $**p \leq 0.01$; $***p \leq 0.001$

expect lower numbers of neurons within the VPL nucleus (for the anatomical location of this nucleus see Fig. 5d, arrow). As shown in Fig. 5e, there was a significant decrease in the numbers of neurons within the VPL nucleus of the thalamus in EAE vs. control treated animals (756.4 ± 285.5 in control animals vs. 648.6 ± 250.1 in EAE animals; $p = 0.0013$). To conclude, neuronal integrity is disturbed despite the absence of inflammatory infiltrates in this region.

Discussion

In this study, we were able to demonstrate that toxin-induced demyelination by feeding mice with the neurotoxin cuprizone induces demyelination and neurodegenerative changes in the thalamus, whereas this interbrain structure is not directly affected in the autoimmune MS animal model EAE (at least if $MOG_{35–55}$ peptide is used in C57BL/6 animals). Furthermore, we were able to demonstrate for the first time that despite the absence of inflammatory lesions within the thalamus, neurodegeneration occurs in this brain structure (i.e., loss of neurons) which might be due to the degeneration of afferent thalamic fiber tracts (i.e., transneuronal degeneration).

Various animal models exist to study MS pathogenesis and concomitant disease progression. Since MS is a very complex and heterogeneous disease, all of these models are valuable and represent important aspects of the human disease. The involvement of the thalamus in MS animal models is, surprisingly, not well studied. In 1971, Kesterson and Carlton described edematous vacuolization, creating spongiform tissue alterations 5 days after initiation of cuprizone intoxication which was widespread but prominent in distinct brain regions, among them the thalamus (Kesterson and Carlton 1971). Since then, the thalamus as a region affected by the cuprizone intoxication received minor attention. Most studies focused on the white matter demyelination in this model. Nevertheless, it is obvious that cuprizone intoxication induces profound cellular changes within the thalamus, such as reduction in oligodendrocyte numbers (Yang et al. 2009), or decreased levels of several metabolites, among N-acetylaspartate (NAA) or N-acetyl-aspartyl-glutamate (Xuan et al. 2014). In this study, we demonstrated that significant demyelination, paralleled by microgliosis and astrogliosis can be seen in the thalamus

after a 5-week cuprizone intoxication period. Furthermore, we did demonstrate the formation of APP^+ spheroids, which is a valid and frequently applied histopathological marker to visualize acute axonal damage in brain tissues.

Accumulation of APP^+ spheroids and reduction of NAA levels both indicate neurodegeneration. NAA is synthesized in neurons through the acetylation by acetyl coenzyme A of free aspartate by the enzyme L-aspartate N-acetyltransferase and catabolized by the enzyme aspartoacylase (ASPA) (Krauspe et al. 2015), which is predominantly expressed in oligodendrocytes. Because, after glutamate, NAA is the second most abundant amino acid in the human central nervous system, its single peak is the most intense in proton magnetic resonance spectroscopy (1H-MRS) of a healthy brain (Rigotti et al. 2007). Reduced levels of NAA indicate axonal degeneration (Bitsch et al. 1999). The NAA-level quantification, as measured by 1H-MRS, is currently the best and most specific noninvasive marker of neuronal and axonal pathology in MS patients (Bjartmar et al. 2000, 2002). Observed reduced NAA levels in the thalamus of cuprizone-exposed animals (Xuan et al. 2014) further support our notion that demyelination and reactive gliosis is paralleled by thalamic neurodegeneration in this model. However, one has to point out that the marker used to visualize thalamic neurodegeneration in this part of the study was accumulation of APP in injured axons. Such axons do either belong to efferent pathways originating from thalamic nuclei or to afferent pathways projecting towards thalamic nuclei. Whether or not there is a decline of neuronal cell body loss in the thalamus itself remains to be clarified for the cuprizone model.

Comparable to the cuprizone model, not much is known about thalamus involvement in EAE models. $MOG_{35–55}$-induced EAE in non-obese diabetic (NOD) mice results in lesions of the thalamus visualized noninvasively by MRI (Levy Barazany et al. 2014). In C57BL/6 $MOG_{35–55}$-induced EAE, it has been observed that mast cells accumulate at the thalamic border (Kim et al. 2010). Similar results have been reported in a rat model where animals have been immunized with spinal cord homogenate (Cook et al. 2000; Dimitriadou et al. 2000). Beyond, increased nerve growth factor levels were found in the thalamus of EAE-diseased rats (Calza et al. 1997; De Simone et al. 1996; Micera et al. 1995). Furthermore, in EAE animals, there were higher thalamic expression levels of the mast cell markers, c-kit, and CD40L, as well as the astrocyte marker GFAP, the later indicating activation of astrocytes. Meuth and colleagues were able to show that neuronal channels regulating the efflux of potassium ions and by this can orchestrate neuronal death through intracellular potassium depletion, are lower expressed in the thalamus of rats undergoing MOG-induced EAE (Meuth et al. 2008). In summary, the thalamus appears to be affected in distinct EAE models; however, such changes are relatively mild as compared to the pronounced pathology observed in other brain regions such as the spinal cord or the cerebellum (Orr et al. 1994; Scheld et al. 2016). These results from various groups are in line with our observations. We were as well able to show that $GFAP^+$ cell number tend to be higher in the thalamus of EAE compared to control mice (active EAE; see Fig. 3). Furthermore, while severe inflammation was present in the spinal cord (compare Fig. 3) and the cerebellum (not shown), such inflammatory changes were not found in the thalamus in animals sacrificed during the peak phase of the disease. The relatively mild loss of oligodendrocytes, together with the moderate activation of microglia at the absence of inflammatory infiltrates and overt demyelinating foci, suggests that such cellular changes are secondary, although this was not directly investigated. However, transneuronal degeneration is well feasible as the underlying mechanism for moderate oligodendrocyte loss and microglia activation in the thalamus after acute EAE.

In support of the assumption that inflammatory demyelination of thalamic afferent pathways induces neuronal degeneration in the thalamus is our observation of neuronal loss in the VPL. Whether or not the intense EAE lesions distant to the thalamus (i.e., within the spinal cord) induce thalamic neurodegeneration by the abovementioned processes was not yet systematically addressed in previous studies. In this study, we were able to show that (i) sensory pathways which project to the thalamus (i.e., the spinothalamic tract) are demyelinated on the spinal cord level and that (ii) this is paralleled by significant neuronal loss in the respective target region which is the ventral posterolateral nucleus of the thalamus (i.e., VPL). Since the thalamus is not directly attacked in the EAE model, indirect mechanisms are most likely operant. Such mechanisms include transneuronal degeneration or disturbed axonal transport [for an extensive review on that topic see (Kipp et al. 2015)]. The term trans-neuronal degeneration describes the death of neurons resulting from the disruption of *input from* or *output to* other nearby neurons. Such damage might occur in an anterograde or retrograde fashion, indicating the direction of the degeneration relative to the original site of damage. Anterograde trans-neuronal degeneration is caused by a loss of input, whereas retrograde trans-neuronal degeneration is damage caused by loss of trophic support from the target.

In our studies, anterograde trans-neuronal degeneration might be operant. We were able to demonstrate that thalamic afferent fiber tracts are demyelinated and display histological evidence for acute axonal damage (i.e., APP accumulation). The loss of spinal cord axons in $MOG_{35–55}$-induced EAE is well in line with findings from other groups (Berard et al. 2010; Herrero-Herranz et al. 2008; Kuerten et al. 2011). In an ultrastructural study, it has been shown that while in acute EAE, histopathology in white matter lesions was characterized by massive immune cell infiltration and tissue edema, inflammatory changes were less pronounced in chronic EAE. In contrast, the later disease stages were dominated by

neurodegenerative changes (Recks et al. 2013). Importantly, the authors noted that axonal pathologies are present from the earliest disease stages on in $MOG_{35–55}$-induced EAE. This observation is well in line with ours. As shown in Fig. 3, animals sacrificed at the peak of the disease display intense APP-spheroid accumulation in the spinal cord white matter.

In summary, the thalamus is presumably directly involved in the disease process induced by global cuprizone intoxication. This means that cuprizone directly attacks oligodendrocytes within the thalamus and, in consequence, induces demyelination, gliosis, and neurodegeneration. In contrast, the thalamus appears not to be directly involved in the disease process in the $MOG_{35–55}$-induced EAE model, but transneuronal degeneration might be operant. Bearing in mind that thalamus atrophy in MS patients might occur either because lesions develop within the thalamus or because of trans-neuronal degeneration, the cuprizone model is a valuable tool to study the first aspect, whereas the EAE model is best suitable to study the later one. Future studies are now warranted to address which mechanisms are operant and how such trans-neuronal deleterious effects can be ameliorated by pharmacological intervention.

Acknowledgments M Kipp and N Wagenknecht received financial support from Novartis/Germany. This study was supported by Novartis Pharma GmbH, Germany.

References

Barnett MH, Prineas JW (2004) Relapsing and remitting multiple sclerosis: pathology of the newly forming lesion. Ann Neurol 55:458–468

Batista S, Zivadinov R, Hoogs M, Bergsland N, Heininen-Brown M, Dwyer MG, Weinstock-Guttman B, Benedict RH (2012) Basal ganglia, thalamus and neocortical atrophy predicting slowed cognitive processing in multiple sclerosis. J Neurol 259:139–146

Benedict RH, Hulst HE, Bergsland N, Schoonheim MM, Dwyer MG, Weinstock-Guttman B, Geurts JJ, Zivadinov R (2013) Clinical significance of atrophy and white matter mean diffusivity within the thalamus of multiple sclerosis patients. Mult Scler 19:1478–1484

Berard JL, Wolak K, Fournier S, David S (2010) Characterization of relapsing-remitting and chronic forms of experimental autoimmune encephalomyelitis in C57BL/6 mice. Glia 58:434–445

Berkley KJ (1986) Specific somatic sensory relays in the mammalian diencephalon. Rev Neurol (Paris) 142:283–290

Bitsch A, Bruhn H, Vougioukas V, Stringaris A, Lassmann H, Frahm J, Bruck W (1999) Inflammatory CNS demyelination: histopathologic correlation with in vivo quantitative proton MR spectroscopy. AJNR Am J Neuroradiol 20:1619–1627

Bitsch A, Schuchardt J, Bunkowski S, Kuhlmann T, Bruck W (2000) Acute axonal injury in multiple sclerosis. Correlation with demyelination and inflammation. Brain 123(Pt 6):1174–1183

Bjartmar C, Kidd G, Mork S, Rudick R, Trapp BD (2000) Neurological disability correlates with spinal cord axonal loss and reduced N-acetyl aspartate in chronic multiple sclerosis patients. Ann Neurol 48:893–901

Bjartmar C, Battistuta J, Terada N, Dupree E, Trapp BD (2002) N-acetylaspartate is an axon-specific marker of mature white matter in vivo: a biochemical and immunohistochemical study on the rat optic nerve. Ann Neurol 51:51–58

Blinkenberg M, Rune K, Jensen CV, Ravnborg M, Kyllingsbaek S, Holm S, Paulson OB, Sorensen PS (2000) Cortical cerebral metabolism correlates with MRI lesion load and cognitive dysfunction in MS. Neurology 54:558–564

Bo L, Geurts JJ, Mork SJ, van der Valk P (2006) Grey matter pathology in multiple sclerosis. Acta Neurol Scand Suppl 183:48–50

Brex PA, Jenkins R, Fox NC, Crum WR, O'Riordan JI, Plant GT, Miller DH (2000) Detection of ventricular enlargement in patients at the earliest clinical stage of MS. Neurology 54:1689–1691

Calabrese M, Rinaldi F, Mattisi I, Bernardi V, Favaretto A, Perini P, Gallo P (2011) The predictive value of gray matter atrophy in clinically isolated syndromes. Neurology 77:257–263

Calabrese M, Magliozzi R, Ciccarelli O, Geurts JJ, Reynolds R, Martin R (2015) Exploring the origins of grey matter damage in multiple sclerosis. Nat Rev Neurosci 16:147–158

Calza L, Giardino L, Pozza M, Micera A, Aloe L (1997) Time-course changes of nerve growth factor, corticotropin-releasing hormone, and nitric oxide synthase isoforms and their possible role in the development of inflammatory response in experimental allergic encephalomyelitis. Proc Natl Acad Sci U S A 94:3368–3373

Cifelli A, Arridge M, Jezzard P, Esiri MM, Palace J, Matthews PM (2002) Thalamic neurodegeneration in multiple sclerosis. Ann Neurol 52:650–653

Clarner T, Janssen K, Nellessen L, Stangel M, Skripuletz T, Krauspe B, Hess FM, Denecke B, Beutner C, Linnartz-Gerlach B, et al. (2015) CXCL10 triggers early microglial activation in the cuprizone model. J Immunol 194:3400–3413

Cook LL, Persinger MA, Koren SA (2000) Differential effects of low frequency, low intensity (<6 mG) nocturnal magnetic fields upon infiltration of mononuclear cells and numbers of mast cells in Lewis rat brains. Toxicol Lett 118:9–19

De Groot CJ, Bergers E, Kamphorst W, Ravid R, Polman CH, Barkhof F, van der Valk P (2001) Post-mortem MRI-guided sampling of multiple sclerosis brain lesions: increased yield of active demyelinating and (p)reactive lesions. Brain 124:1635–1645

De Simone R, Micera A, Tirassa P, Aloe L (1996) mRNA for NGF and p75 in the central nervous system of rats affected by experimental allergic encephalomyelitis. Neuropathol Appl Neurobiol 22:54–59

Derache N, Marie RM, Constans JM, Defer GL (2006) Reduced thalamic and cerebellar rest metabolism in relapsing-remitting multiple sclerosis, a positron emission tomography study: correlations to lesion load. J Neurol Sci 245:103–109

Dieni S, Matsumoto T, Dekkers M, Rauskolb S, Ionescu MS, Deogracias R, Gundelfinger ED, Kojima M, Nestel S, Frotscher M, et al. (2012) BDNF and its pro-peptide are stored in presynaptic dense core vesicles in brain neurons. J Cell Biol 196:775–788

Dimitriadou V, Pang X, Theoharides TC (2000) Hydroxyzine inhibits experimental allergic encephalomyelitis (EAE) and associated brain mast cell activation. Int J Immunopharmacol 22:673–684

Dutta R, Trapp BD (2014) Relapsing and progressive forms of multiple sclerosis: insights from pathology. Curr Opin Neurol 27:271–278

Ferguson IA, Schweitzer JB, Johnson EM Jr (1990) Basic fibroblast growth factor: receptor-mediated internalization, metabolism, and anterograde axonal transport in retinal ganglion cells. J Neurosci 10:2176–2189

Figueiredo C, Pais TF, Gomes JR, Chatterjee S (2008) Neuron-microglia crosstalk up-regulates neuronal FGF-2 expression which mediates neuroprotection against excitotoxicity via JNK1/2. J Neurochem 107:73–85

Gilbert JJ, Sadler M (1983) Unsuspected multiple sclerosis. Arch Neurol 40:533–536

Goldberg J, Daniel M, van Heuvel Y, Victor M, Beyer C, Clarner T, Kipp M (2013) Short-term cuprizone feeding induces selective amino

acid deprivation with concomitant activation of an integrated stress response in oligodendrocytes. Cell Mol Neurobiol 33:1087–1098

Herrero-Herranz E, Pardo LA, Gold R, Linker RA (2008) Pattern of axonal injury in murine myelin oligodendrocyte glycoprotein induced experimental autoimmune encephalomyelitis: implications for multiple sclerosis. Neurobiol Dis 30:162–173

Houtchens MK, Benedict RH, Killiany R, Sharma J, Jaisani Z, Singh B, Weinstock-Guttman B, Guttmann CR, Bakshi R (2007) Thalamic atrophy and cognition in multiple sclerosis. Neurology 69:1213–1223

Inglese M, Park SJ, Johnson G, Babb JS, Miles L, Jaggi H, Herbert J, Grossman RI (2007) Deep gray matter perfusion in multiple sclerosis: dynamic susceptibility contrast perfusion magnetic resonance imaging at 3 T. Arch Neurol 64:196–202

Jones EG (1991) The anatomy of sensory relay functions in the thalamus. Prog Brain Res 87:29–52

Kesterson JW, Carlton WW (1971) Histopathologic and enzyme histochemical observations of the cuprizone-induced brain edema. Exp Mol Pathol 15:82–96

Kim DY, Jeoung D, Ro JY (2010) Signaling pathways in the activation of mast cells cocultured with astrocytes and colocalization of both cells in experimental allergic encephalomyelitis. J Immunol 185:273–283

Kipp M, Clarner T, Dang J, Copray S, Beyer C (2009) The cuprizone animal model: new insights into an old story. Acta Neuropathol 118: 723–736

Kipp M, Gingele S, Pott F, Clarner T, van der Valk P, Denecke B, Gan L, Siffrin V, Zipp F, Dreher W, et al. (2011) BLBP-expression in astrocytes during experimental demyelination and in human multiple sclerosis lesions. Brain Behav Immun 25:1554–1568

Kipp M, van der Valk P, Amor S (2012) Pathology of multiple sclerosis. CNS Neurol Disord Drug Targets 11:506–517

Kipp M, Wagenknecht N, Beyer C, Samer S, Wuerfel J, Nikoubashman O (2015) Thalamus pathology in multiple sclerosis: from biology to clinical application. Cell Mol Life Sci 72:1127–1147

Krauspe BM, Dreher W, Beyer C, Baumgartner W, Denecke B, Janssen K, Langhans CD, Clarner T, Kipp M (2015) Short-term cuprizone feeding verifies N-acetylaspartate quantification as a marker of neurodegeneration. J Mol Neurosci 55:733–748

Kuerten S, Gruppe TL, Laurentius LM, Kirch C, Tary-Lehmann M, Lehmann PV, Addicks K (2011) Differential patterns of spinal cord pathology induced by MP4, MOG peptide 35-55, and PLP peptide 178-191 in C57BL/6 mice. APMIS 119:336–346

Levy Barazany H, Barazany D, Puckett L, Blanga-Kanfi S, Borenstein-Auerbach N, Yang K, Peron JP, Weiner HL, Frenkel D (2014) Brain MRI of nasal MOG therapeutic effect in relapsing-progressive EAE. Exp Neurol 255C:63–70

Lublin FD, Reingold SC (1996) Defining the clinical course of multiple sclerosis: results of an international survey. National Multiple Sclerosis Society (USA) Advisory Committee on Clinical Trials of New Agents in Multiple Sclerosis. Neurology 46:907–911

Lucchinetti C, Bruck W, Parisi J, Scheithauer B, Rodriguez M, Lassmann H (2000) Heterogeneity of multiple sclerosis lesions: implications for the pathogenesis of demyelination. Ann Neurol 47:707–717

Magon S, Chakravarty MM, Amann M, Weier K, Naegelin Y, Andelova M, Radue EW, Stippich C, Lerch JP, Kappos L and others. 2014. Label-fusion-segmentation and deformation-based shape analysis of deep gray matter in multiple sclerosis: The impact of thalamic subnuclei on disability. Hum Brain Mapp

Marik C, Felts PA, Bauer J, Lassmann H, Smith KJ (2007) Lesion genesis in a subset of patients with multiple sclerosis: a role for innate immunity? Brain 130:2800–2815

McCabe BD, Marques G, Haghighi AP, Fetter RD, Crotty ML, Haerry TE, Goodman CS, O'Connor MB (2003) The BMP homolog Gbb provides a retrograde signal that regulates synaptic growth at the Drosophila neuromuscular junction. Neuron 39:241–254

McFarland NR, Haber SN (2002) Thalamic relay nuclei of the basal ganglia form both reciprocal and nonreciprocal cortical connections, linking multiple frontal cortical areas. J Neurosci 22:8117–8132

Meuth SG, Kanyshkov T, Melzer N, Bittner S, Kieseier BC, Budde T, Wiendl H (2008) Altered neuronal expression of TASK1 and TASK3 potassium channels in rodent and human autoimmune CNS inflammation. Neurosci Lett 446:133–138

Micera A, De Simone R, Aloe L (1995) Elevated levels of nerve growth factor in the thalamus and spinal cord of rats affected by experimental allergic encephalomyelitis. Arch Ital Biol 133:131–142

Minagar A, Barnett MH, Benedict RH, Pelletier D, Pirko I, Sahraian MA, Frohman E, Zivadinov R (2013) The thalamus and multiple sclerosis: modern views on pathologic, imaging, and clinical aspects. Neurology 80:210–219

Mosca TJ, Hong W, Dani VS, Favaloro V, Luo L (2012) Trans-synaptic Teneurin signalling in neuromuscular synapse organization and target choice. Nature 484:237–241

Nikoletopoulou V, Lickert H, Frade JM, Rencurel C, Giallonardo P, Zhang L, Bibel M, Barde YA (2010) Neurotrophin receptors TrkA and TrkC cause neuronal death whereas TrkB does not. Nature 467: 59–63

Orr EL, Aschenbrenner JE, Oakford LX, Jackson FL, Stanley NC (1994) Changes in brain and spinal cord water content during recurrent experimental autoimmune encephalomyelitis in female Lewis rats. Mol Chem Neuropathol 22:185–195

Ota M, Sato N, Nakata Y, Ito K, Kamiya K, Maikusa N, Ogawa M, Okamoto T, Obu S, Noda T, et al. (2013) Abnormalities of cerebral blood flow in multiple sclerosis: a pseudocontinuous arterial spin labeling MRI study. Magn Reson Imaging 31:990–995

Purves D, Snider WD, Voyvodic JT (1988) Trophic regulation of nerve cell morphology and innervation in the autonomic nervous system. Nature 336:123–128

Rashid W, Parkes LM, Ingle GT, Chard DT, Toosy AT, Altmann DR, Symms MR, Tofts PS, Thompson AJ, Miller DH (2004) Abnormalities of cerebral perfusion in multiple sclerosis. J Neurol Neurosurg Psychiatry 75:1288–1293

Recks MS, Stormanns ER, Bader J, Arnhold S, Addicks K, Kuerten S (2013) Early axonal damage and progressive myelin pathology define the kinetics of CNS histopathology in a mouse model of multiple sclerosis. Clin Immunol 149:32–45

Rigotti DJ, Inglese M, Gonen O (2007) Whole-brain N-acetylaspartate as a surrogate marker of neuronal damage in diffuse neurologic disorders. AJNR Am J Neuroradiol 28:1843–1849

Rocca MA, Mesaros S, Pagani E, Sormani MP, Comi G, Filippi M (2010) Thalamic damage and long-term progression of disability in multiple sclerosis. Radiology 257:463–469

Ruffini F, Rossi S, Bergamaschi A, Brambilla E, Finardi A, Motta C, Studer V, Barbieri F, De Chiara V, Hayardeny L, et al. (2013) Laquinimod prevents inflammation-induced synaptic alterations occurring in experimental autoimmune encephalomyelitis. Mult Scler 19:1084–1094

Scheld M, Ruther BJ, Grosse-Veldmann R, Ohl K, Tenbrock K, Dreymuller D, Fallier-Becker P, Zendedel A, Beyer C, Clarner T, et al. (2016) Neurodegeneration triggers peripheral immune cell recruitment into the forebrain. J Neurosci 36:1410–1415

Schmidt T, Awad H, Slowik A, Beyer C, Kipp M, Clarner T (2013) Regional heterogeneity of cuprizone-induced demyelination: topographical aspects of the midline of the corpus callosum. J Mol Neurosci 49:80–88

Schoonheim MM, Popescu V, Rueda Lopes FC, Wiebenga OT, Vrenken H, Douw L, Polman CH, Geurts JJ, Barkhof F (2012) Subcortical atrophy and cognition: sex effects in multiple sclerosis. Neurology 79:1754–1761

Sherman SM (2007) The thalamus is more than just a relay. Curr Opin Neurobiol 17:417–422

Shipp S (2003) The functional logic of cortico-pulvinar connections. Philos Trans R Soc Lond Ser B Biol Sci 358:1605–1624

Skripuletz T, Gudi V, Hackstette D, Stangel M (2011) De- and remyelination in the CNS white and grey matter induced by cuprizone: the old, the new, and the unexpected. Histol Histopathol 26:1585–1597

Skripuletz T, Hackstette D, Bauer K, Gudi V, Pul R, Voss E, Berger K, Kipp M, Baumgartner W, Stangel M (2013) Astrocytes regulate myelin clearance through recruitment of microglia during cuprizone-induced demyelination. Brain 136:147–167

Skripuletz T, Manzel A, Gropengiesser K, Schafer N, Gudi V, Singh V, Salinas Tejedor L, Jorg S, Hammer A, Voss E, et al. (2015) Pivotal role of choline metabolites in remyelination. Brain 138:398–413

Slowik A, Schmidt T, Beyer C, Amor S, Clarner T, Kipp M (2015) The sphingosine 1-phosphate receptor agonist FTY720 is neuroprotective after cuprizone-induced CNS demyelination. Br J Pharmacol 172:80–92

Sommer MA (2003) The role of the thalamus in motor control. Curr Opin Neurobiol 13:663–670

Soulika AM, Lee E, McCauley E, Miers L, Bannerman P, Pleasure D (2009) Initiation and progression of axonopathy in experimental autoimmune encephalomyelitis. J Neurosci 29:14965–14979

Stromnes IM, Goverman JM (2006) Passive induction of experimental allergic encephalomyelitis. Nat Protoc 1:1952–1960

Vercellino M, Masera S, Lorenzatti M, Condello C, Merola A, Mattioda A, Tribolo A, Capello E, Mancardi GL, Mutani R, et al. (2009) Demyelination, inflammation, and neurodegeneration in multiple sclerosis deep gray matter. J Neuropathol Exp Neurol 68:489–502

Xuan Y, Yan G, Peng H, Wu R, Xu H (2014) Concurrent changes in (1)H MRS metabolites and antioxidant enzymes in the brain of C57BL/6 mouse short-termly exposed to cuprizone: possible implications for schizophrenia. Neurochem Int 69:20–27

Yang HJ, Wang H, Zhang Y, Xiao L, Clough RW, Browning R, Li XM, Xu H (2009) Region-specific susceptibilities to cuprizone-induced lesions in the mouse forebrain: implications for the pathophysiology of schizophrenia. Brain Res 1270: 121–130

Zivadinov R, Havrdova E, Bergsland N, Tyblova M, Hagemeier J, Seidl Z, Dwyer MG, Vaneckova M, Krasensky J, Carl E, et al. (2013) Thalamic atrophy is associated with development of clinically definite multiple sclerosis. Radiology 268: 831–841